Check for updates

Uncovering friction dynamics using hydrogel particles as soft ball bearings

Raisa E. D. Rudge, [ab] Jesse P. M. van de Sande,[a] Joshua A. Dijksman [b] and Elke Scholten*[a]

Rolling ball bearings are widely known and applied to decrease friction between two surfaces. More recently, hydrogel–hydrogel tribopairs have also revealed good but rather complex lubrication properties. Here, we use hydrogels as ball bearings to elucidate that soft spherical particles have nontrivial rate-dependent lubrication behavior. Unlike Newtonian lubrication or dry solid friction, hydrogel particles in suspension transition through four frictional regimes as a function of sliding velocity. We relate the different regimes to the deformation of the particles at different gap sizes, which changes the effective contact area between the sliding surfaces. By systematically varying the particle characteristics and the surface properties of the sliding surfaces, we assign potential mechanisms for each of the different lubricating regimes as a function of velocity: (I) relatively high friction due to particle flattening and direct contact between interacting bodies (II) decrease of friction owing to the presence of rolling particles (III) large inflow of particles in a confined space leading to compressed particles and (IV) the formation of a thick lubricating layer. Using these suspensions with soft, deformable particles as a ball bearing system, we provide new insights into soft material friction with applications in emulsions, powders, pastes or other granular materials.

1 Introduction

Friction is of importance for the functionality of many different mechanical systems such as car tires, steel bearings, biomedical implants and even human joints. The friction coefficient expresses the ease with which two surfaces slide alongside one another and is calculated from the friction force (F_F) and the normal force (F_N) as $\mu = F_F/F_N$. There are numerous parameters known to influence friction between two surfaces. As such, μ can depend on velocity, normal force, adhesion, roughness *etc.* A simple strategy to obtain low friction is to keep sliding surfaces from physically touching each other. It should be noted that low friction can also be obtained when surfaces are in contact with one another. In the case of hydrogels, it has been shown that a decrease in friction can be obtained with increased contact areas.[1,2] To decrease the high frictional values caused by increased contact, the contact area between surfaces in motion can be minimized in many ways. The simple presence of a thin lubricating fluid layer or polymer coating can already decrease the friction coefficient by orders of magnitude by preventing the surfaces to come into direct contact.[3,4] Additionally, solid spheres are able to decrease friction (Fig. 1a). Solid spheres

between two sliding surfaces have the ability to decrease friction by separating the sliding surfaces. Although the spheres themselves are in direct contact with both surfaces, their ability to roll provides a lubrication mechanism. This is known as the ball bearing mechanism[5–7] or third body friction[8] and this mechanism plays an important role in most machinery with rotating parts and can be found in applications from kitchen appliances[9] to
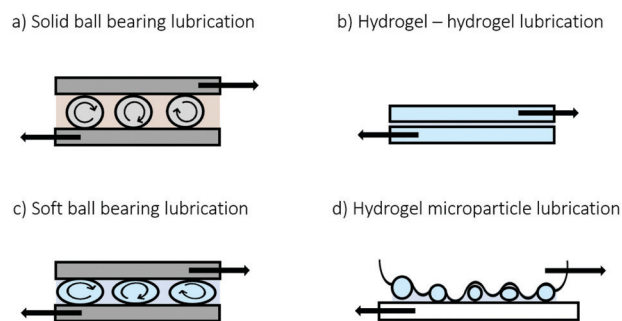

Fig. 1 Examples of frictional mechanisms for different combinations of surfaces and lubricants. (a) The traditional solid ball bearing lubrication involves rolling spheres between hard surfaces, sometimes grease-lubricated. (b) Hydrogel–hydrogel friction with two hydrogels sliding directly against one another. There is commonly a thin layer of water present between the soft surfaces. (c) Hydrogel spheres as soft ball bearings. Here deformability strongly influences friction coefficient. (d) Hydrogel particles in contact with a hard/soft rough surface.

[a] *Physics and Physical Chemistry of Foods, Wageningen University, The Netherlands. E-mail: elke.scholten@wur.nl*

[b] *Physical Chemistry and Soft Matter, Wageningen University, The Netherlands*

space crafts.[10] Due to the smoothness of the sphere's surface, the presence of rolling bearings can reduce the friction coefficient much more compared to sliding surfaces in direct contact.[11] By using ball bearings that by themselves already provide very low (rate-dependent) friction, one can ask how the bearing contact friction affects the ball bearing mechanism. Additionally, ball bearing or substrate deformation is often not considered in ball bearing mechanisms, as ball bearings are typically stressed much below their internal strength. Deformation of ball bearings might significantly affect the involved contact areas, and with that lubrication behavior of ball bearings. For soft, slippery ball bearings we can thus expect nontrivial lubrication behavior.

To explore this potentially nontrivial lubrication behavior, we consider hydrogels as soft ball bearings. Hydrogels have become immensely popular in the past decades and these materials have, more recently, been the subject of a broad range of frictional studies.[1,12–15] Hydrogels exhibit unique frictional behavior and friction coefficients as low as 0.01 have been reported for hydrogel-on-hydrogel friction (Fig. 1b).[2,16] This is similar to friction coefficients in synovial joints. The exact mechanism by which these low friction coefficients in hydrogels come about is still under debate with many proposed mechanisms.[13,17–20]

Here, we present a hybrid lubricant that combines the rolling ability of spherical particles with the slipperiness of hydrogels (Fig. 1c) and show that using soft hydrogel particles as ball bearings indeed induces unique lubricating properties. We use a suspension containing gelatin microparticles as a lubricant. These gelatin microparticles allow us to easily tune the frictional behavior by varying the particle properties, such as particle deformability and size. We show that when combined with real-life rough surfaces (Fig. 1d), soft slippery ball bearings bring an additional lubrication effect. By systematically exploring the role of different particle characteristics, we elucidate the microscopic mechanism behind the lubricating behavior of soft hydrogel suspensions.

Particle suspensions have been studied before for their lubricating efficiency. Previous studies have addressed the effect of polymer content of the lubricating particles,[21] particle volume fraction in suspension,[22] along with changes in the continuous phase[23,24] and the tribopairs used.[25] From these studies it becomes evident that hydrogel particles enhance the lubrication behavior over a range of velocities and past authors have proposed several different mechanisms to interpret their findings. While it was suggested that the particles are not yet present between the surfaces at low velocities,[21,26] this interpretation contradicts findings of other authors.[27] The different results obtained by various authors may be in part due to the use of different tribometers and different types of particles. As a tribological measurement strongly depends on the properties of the entire system (measuring device, lubricant type, velocity *etc.*),[28,29] comparing results of different studies is often difficult.

In the present work, we present a systematic study highlighting the rate-dependent dynamics of hydrogel ball bearing lubrication. We vary the volume fraction of the particles in suspension, the deformability of the hydrogel particles, and the particle size, and ensure that all measurements are carried out under the same conditions. In addition, we show the importance of the surface roughness of the interacting surfaces on the frictional behavior over a range of velocities. Our soft particles show frictional behavior that deviates from fluid lubricated systems as commonly described by means of a Stribeck curve which predicts a boundary, mixed and hydrodynamic regime.[11] In the case of particle suspensions, four or even more frictional regimes can be observed.[21,28] The exact mechanisms behind the frictional behaviour of soft particle suspensions are however not fully understood.[26,28,30]

To contribute to a better general understanding of soft particle lubrication, we introduce gelatin microparticles as soft ball bearing spheres. The deformability of our particles introduces the four rate-dependent regimes. We discuss possible underlying mechanisms for the different regimes. Overall, our soft sphere suspensions show that limited contact between the sliding surfaces gives rise to easy sliding and low friction coefficients. This is the case for high volume fraction suspensions, hard particles and large particles, as these samples are well able to separate the sliding surfaces. The suspension of soft spherical particles we introduced can function as a model system to thoroughly understand the frictional behavior of powders, pastes and suspensions commonly used in agriculture, pharmaceutics and foods.

2 Experimental

2.1 Gelatin microparticle preparation

We use gelatin microparticles (Fig. 2) as our soft hydrogel ball bearings. To obtain the gelatin microparticles, we first make gelatin solutions of the relevant weight percentages (w/w%).

This is done by adding gelatin powder (Type A, Sigma Aldrich) to Milli-Q water. The mixture was shaken and left at room temperature to allow the gelatin powder to hydrate before the mixture was heated to 60 °C to dissolve the gelatin. The gelatin solution was then added in a 1 : 4 ratio to a mixture of sunflower oil and 2.5 wt% emulsifier polyglycerol polyricinoleate (PGPR) at 60 °C. A gelatin solution-in-oil emulsion was created by premixing the gelatin solution with the oil/PGPR mixture for 15 minutes using a magnetic stirring bar. The pre-mixed emulsion was further homogenized using rotor stator homogenization (IKA Ultra Turrax) after which the emulsion was immediately cooled down in an ice bath to induce gelation of the gelatin and create the solid-like hydrogel particles. Mixing time and mixing speed were varied to alter the droplet size. A complete overview of the mixing times and speeds used for each sample can be found in Table 1.
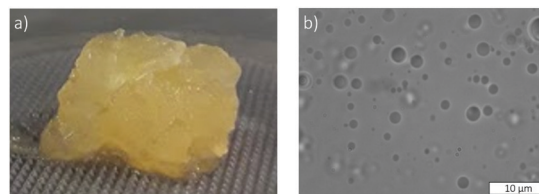

Fig. 2 (a) Densely packed ("100%") gelatin microparticle suspension made with 15 weight% gelatin placed on a 50 mm serrated rheometer plate. (b) Microscopic image of diluted gelatin microparticle suspension in water.

Table 1 An overview of the characteristics of the hydrogel microparticle suspension preparation for suspensions varying in particle content, particle deformability (Young's modulus) and particle size

Sample	Gelatin concentration (wt%)	Young's modulus (kPa)	Mixing time and speed
Microparticle content			
"100%"	15	150	10 min, 6000 rpm
"50%"	15	150	10 min, 6000 rpm
"25%"	15	150	10 min, 6000 rpm
"10%"	15	150	10 min, 6000 rpm
Microparticle deformability			
YM50	10	50	10 min, 6000 rpm
YM90	15	90	10 min, 6000 rpm
YM150	20	150	10 min, 6000 rpm
YM500	15 (chemically cross-linked)	500	10 min, 6000 rpm
Microparticle size			
Small	15	150	15 min, 20 000 rpm
Medium	15	150	10 min, 6000 rpm
Large	15	150	5 min, 500 rpm

To collect the gelatin hydrogel particles, the bulk amount of oil was removed by centrifugation for one cycle of 30 minutes at 16 000 rpm at 4 °C. The residual oil was removed by dispersing the gelatin microparticles in acetone overnight. Acetone with the dissolved oil was removed by filtration, and further drying by air resulted in a dry powder. To prepare the hydrogel particle suspensions, dried particle powder was added to an excess of water to rehydrate the particles. The rehydration returns the particles to their original spherical shape and can be done repeatedly. To avoid agglomeration of the hydrogel particles, we homogenized the suspension for 1 minute using an IKA Ultra Turrax and then for four cycles (one cycle at 40 bar followed by three cycles at 80 bar) using a LAB Homogeniser (Delta Instruments). We confirm the particles remained spherical after treatment, using brightfield microscopy (Fig. 2b). To further increase the hardness of certain microgel particles, we chemically cross-linked gelatin using the treatment described in previously published work.[2] After filtration, we obtained a densely packed hydrogel particle suspension, which was used for rheological and tribological measurements. We refer to this densely packed suspension as "100%", which refers here to maximum packing. The actual volume fraction of particles is much lower, as the maximum packing of spherical, monodisperse particles is theoretically between 64 and 74%.[31] In reality, due to the polydisperse and deformable nature of the particles, the volume fraction may be slightly higher; we hence refrain from making claims about the specific value of the packing fraction and label it as "100%". This densely packed 100% suspension is diluted with Milli-Q water to obtain 50%, 25% and 10% of the maximum packing by weight.

2.2 Young's moduli

The stiffness of the microparticles was estimated by measuring the elastic modulus of macroscopic gels, assuming that the properties of the gels at the two different length scales are comparable.

Gelatin gels with the same ingredients as used for the particles were cut into disks of 26 mm in diameter with a height of 20 mm. A uni-axial compression was performed using a TA.XT Plus Texture analyser (Stable Micro Systems Ltd) loaded with a 50 kg load cell and equipped with a disk-shaped acrylic indentor of 100 mm diameter moving at a speed of 1 mm s^{-1}. We determined the stress–strain ratio in the linear regime to obtain the Young's modulus for samples of 5, 10, 15, 20 and 25% of gelatin.

2.3 Particle size

The size distribution and polydispersity of the gelatin hydrogel microparticles were investigated using static light scattering (Malvern Mastersizer 2000). The average particle size was determined by the volume-weighted mean which is referred to as the $D[4,3]$ value. Additionally, particle shape and size were examined using bright-field optical microscopy (Zeiss Axioskop 50 + AxioCam HRc) with a 63× objective oil lens. To obtain clear and informative microscopy images, the samples were diluted with MilliQ water with a dilution ratio of 1 : 9 as displayed in Fig. 2b.

2.4 Rheological properties

The rheological properties of the densely packed hydrogel particle suspensions were determined using an Anton Paar MCR 502 Rheometer equipped with a plate-plate geometry (measuring plate PP50/P2 profiled 1 × 0.5 and inset 50 mm profiled plate) at 20 °C. Serrated plates were used to reduce the influence of wall slip. The sample was placed on the serrated plate and the viscosity was measured as a function of decreasing shear rate of 100–0.1 s^{-1} (logarithmic ramp) during 468 seconds.

2.5 Tribological properties

The tribological properties of densely packed gelatin hydrogel particle suspensions were investigated using an Anton Paar MCR 302 rheometer with a tribocell setup (measuring shaft BC 12.7 with a spherical glass probe of diameter 12.7 mm) and three cylindrical polydimethylsiloxane (PDMS) substrates (diameter: 6 mm, height: 6 mm) as schematically displayed in Fig. 3. The rough surface of the glass probe has asperities of sizes ranging between 10 and 100 micrometers as visualized using a light microscope (displayed in Section 3.4.1 Surface–particle interactions). From atomic force microscopy (AFM) measurements, we estimate the surface asperities of the PDMS substrate to be well below 1 micrometer. Our measurements were performed at a fixed normal load of 1 N and a temperature of 20 °C. Using these settings we ensure that the hydrogel particles do not melt or fracture. At this normal force, the diameter of the contact area is estimated to be 2.2 mm using Hertzian contact mechanics for a spherical object with a modulus of 50 GPa and a flat plane with a modulus of 3 MPa. The corresponding contact pressure is then around 0.4 MPa.

Each measurement consisted of four measuring intervals, in which the rotation speed was logarithmically increased from 0.1 to 1000 rpm (approximately 0.05 to 500 mm s^{-1}) in the first and third interval and decreased from 1000 to 0.1 rpm in the second and fourth interval, respectively. The duration of one
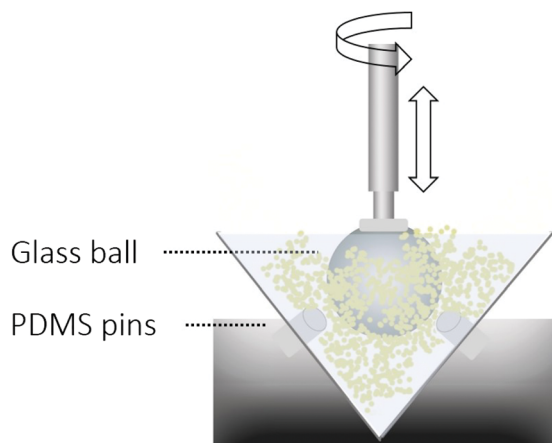
Fig. 3 Anton Paar tribocell equipped with a rough glass ball rotating against flat PDMS pins. The sample is placed in the cup and the velocity and normal force are controlled and monitored. The friction coefficient is obtained from the ratio between the friction force and the normal force as described in eqn (1).
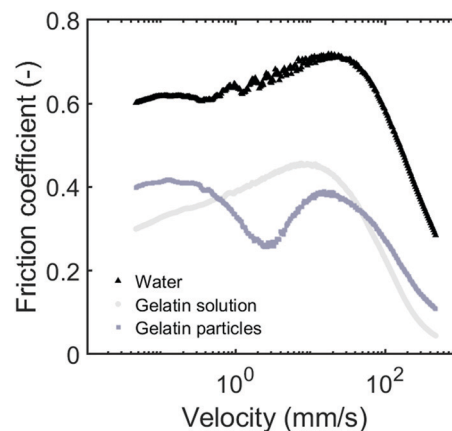

Fig. 4 Lubrication properties of water, a suspension containing hydrogel particles and a gelatin solution with the same dry gelatin content as the particle suspension. Frictional measurements were performed between a glass probe and PDMS substrates at increasing velocity.

interval was 300 s, a complete measurement thus lasted 1200 s. The friction coefficient (μ) is determined using the frictional force (F_F) and the normal force (F_N) as shown in eqn (1).

$$\mu = F_F/F_N \qquad (1)$$

The results of the first interval consistently deviated from those from subsequent intervals. This is likely because the sample was not fully entrained between the surfaces or because the system had simply not arrived at an equilibrium state. The results of the first interval were therefore discarded, and only results from the second, third and fourth interval were used for data analysis as these intervals were highly reproducible. The samples were measured in triplicate. Results of particle suspensions presented in the same data set are measured with the same PDMS and glass probe pairs to minimize the effect of small differences in the (surface) properties of the probe and the substrates.

3 Results

To explore the lubrication properties of soft particles between relatively hard surfaces, we use hydrogel microparticle suspensions. We measure the friction coefficients using a tribometer equipped with a glass ball and polydimethylsiloxane (PDMS) pins. We first show friction curves for our suspensions at maximum packing fraction, here referred to as 100% (Fig. 4). The particles in the suspension contained 15% gelatin and had an average particle size of 8 μm. We compare our gelatin particle suspension to a gelatin solution containing the same total gelatin concentration. Both the gelatin solution and the gelatin particle suspension give much lower friction coefficients than water. Gelatin can, both in the form of a biopolymer solution and as a solid particle suspension, reduce the friction coefficient efficiently. This is not surprising, as biopolymer solutions are known to give low friction coefficients.[2,13,32–34] As can be seen, the friction coefficients for both gelatin samples are similarly low, although the shape of the curves are rather different.

Differences in friction coefficient can sometimes be driven by viscosity. The particle suspension in general has a rate-dependent viscosity; at a shear rate of 1 s^{-1} the viscosity is 12.5 Pa s^{-1}, and the gelatin solution has a viscosity of 12 mPa s at the same shear rate. Although the viscosities of both gelatin samples are very different, the samples show similar friction coefficients. Similarly, although the viscosity of the gelatin solution (12 mPa s) is relatively close to that of water (1 mPa s[35]) the friction coefficients are very different. The differences in friction coefficients are clearly not simply a result of the difference in viscosity of the samples.

3.1 Comparing fluid to suspension lubrication

The gelatin solution presumably lowers friction simply by forming a thin, hydrated lubricating layer that is able to keep the surfaces from directly interacting. The particle suspension however, is expected to lubricate the surfaces by means of a ball bearing mechanism where the individual hydrogel particles roll while collectively sustaining the load and keeping the surfaces apart (Fig. 1). For the hydrogel particle suspension, we find that the friction coefficient transitions through multiple regimes. These regimes go beyond the expected boundary, mixed and hydrodynamic regimes for most fluid lubricants, as also seen for the gelatin solution. For our particle suspensions, the friction coefficient is initially rather constant as expected in the boundary regime. We then find a decrease in friction with increased speed, followed by an increase in the friction coefficient upon further increasing the velocity up until around 2 mm s^{-1}. The steep decrease after 20 mm s^{-1} again resembles typical Stribeck behavior in the mixed regime; a strong decrease in friction is seen as the thickness of the lubricating layer increases. At the maximum velocity of 500 mm s^{-1}, the system still appears to be in the mixed regime. If the system had entered the hydrodynamic regime, an increase in friction coefficient would be expected. These velocity dynamics highlight the complexity of lubricants containing soft ball bearings. Similar frictional regimes have been found for other soft

Table 2 Gelatin microparticle characteristics for the different samples used. For the deformability series, YM refers to the Young's modulus of the macroscopic gelatin disks in kPa. The viscosity (Pa s) of the suspensions at a fixed shear rate of 1 s^{-1} is also shown here

Sample	Gelatin concentration (wt%)	Particle size D[4,3] (µm)	Viscosity (Pa s) at shear rate 1 s^{-1}
Microparticle content			
"100%"	15	8	12.5
Microparticle deformability			
YM50	10	6	0.1
YM90	15	8	12.5
YM150	20	11.2	127.7
YM500	15	8	76.5
Microparticle size			
Small	15	12	16
Medium	15	33	12.5
Large	15	150	20

dispersed systems, such as agar particles and whey protein solutions.[21,26,28] In these works, the frictional regimes were suggested to originate from the different fluid or gel particles entering the gap separately at specific velocities. In the boundary regime, at low velocities, it is expected that only fluids or small hydrocolloids are able to enter the gap.[21,26,36] As the velocity increases, the gap size is also thought to increase, and once the gap size increases beyond a critical gap size, particle begin to enter the contact zone.[6,30,37,38] This may initially lead to an increase in friction due to decreased mobility of the two surfaces. Once the lubricant is able to form a uniform layer, the friction decreases steeply as one would expect in the mixed regime.

The descriptions found in literature as summarized above do not fully capture the behavior we find for our gelatin particle suspensions. We find different friction coefficients for all of our samples in the boundary regime as will be described in following sections. Our results indicate that particles are already present in the gap at low velocities, suggesting that the mechanisms currently described in literature are unable to explain the dynamics in our soft hydrogel lubricant. By varying the particle volume fraction, particle deformability and size of the particles we will now systematically investigate the main contributors to the frictional behavior of soft ball bearings. An overview of the hydrogel microparticle suspensions that will be described in the following sections are displayed in Table 2.

3.2 Particle packing fraction

Friction coefficients are expected to be lowest when direct contact between interacting surfaces is minimized. For (semi-)solid spheres as ball bearings, varying the number of spheres separating the surfaces would thus be an efficient way to influence the friction coefficient. We vary the volume fraction of particles present in the suspension to study the effect of particle number on the lubricating ability of soft spheres. The particles used contained 15% gelatin and had an average particle size of 8 µm. A densely packed suspension with maximum packing fraction was obtained by removing as much water as possible by means of centrifugation and subsequent draining of the fluid suspension through a filter.

Fig. 5 shows the friction coefficients measured for the different volume fractions. The sample with the highest volume fraction of hydrogel particles, "100%", gives the lowest friction coefficients if we take all regimes into account. When the volume fraction decreases, the maximum friction coefficient increases from μ_{max} = 0.42 for the 100% samples to μ_{max} = 0.53 for the 10% sample. An increase in friction coefficient with a decrease in particle volume fraction has also been found previously for whey protein particles, which were made by fracturing hydrogels using a hand blender.[22] This increase in friction coefficient with decreasing particle volume fraction is not surprising as the particles are largely responsible for keeping the surfaces separated. With a decreasing volume fraction, the friction coefficient is mostly determined by the lubricating ability of water. As water has a low affinity for the hydrophobic PDMS interface, the measured friction coefficients become as high as 0.7 for pure water (Fig. 4). When diluting the particle suspension to 10% particles, the viscosity decreases more than 600 times compared to the original densely packed suspension. The difference in frictional behavior cannot be explained by this large decrease in viscosity as was also seen in the previous section. It thus appears that the friction coefficient is a result of the lubricating ability of the ball bearing particles and not the viscosity.

In the previous sections we have shown that the hydrogel particle suspensions transition through multiple frictional regimes, especially at high particle volume fractions (Fig. 5).
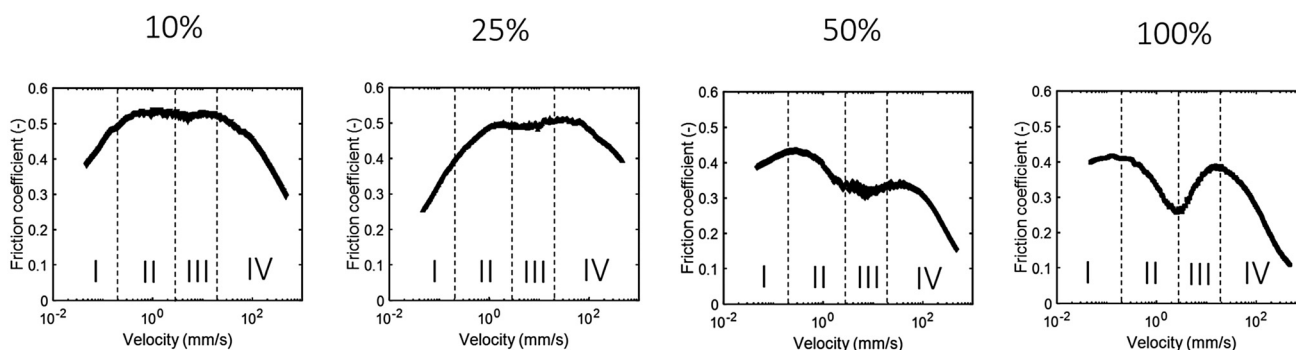

Fig. 5 Tribological behavior of densely packed suspensions (100%) and suspensions diluted to 50%, 25% and 10%.
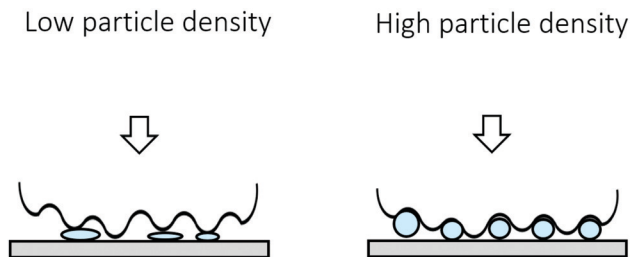
Low particle density   High particle density

Fig. 6 A comparison between low particle volume fractions and high particle volume fractions. At low volume fractions the load per particle is relatively high leading to geometrical deformations of the particles. At higher volume fractions the load per particle is relatively low and particles retain their spherical shape.

Fig. 7 (a) Young's moduli of physically cross-linked gelatin gels at different concentration. (b) Flow curves of microparticle suspensions of particles with different Young's moduli. (c) The friction curves for particles of Young's moduli 50, 90, 150 kPa physically cross-linked gelatin and 500 kPa chemically cross-linked gelatin. (d) A temperature sweep of particles of 90 kPa at 50 mm s^{-1} is shown in panel (d).

At lower volume fractions, the four regimes are less easy to distinguish. Particularly, the separation between the second and third regime becomes less obvious and the drop in the friction coefficient in the second frictional regime decreases. This can be explained by the deformable nature of the particles. The applied load, the same in all experiments, is divided over the present particles. As the number of particles decreases, the load on each individual particle increases proportionally. Such a higher load would cause a higher degree of deformation of the gelatin hydrogel particles, leading to a lower ability of the particles to separate the surfaces and to roll. This decreased rolling ability and a smaller gap size leads to more asperity contact between the surfaces, which explains the higher friction coefficients for suspensions with a lower volume fraction of soft hydrogel particles (Fig. 6). The deformability of the particles therefore seem to play an important role in the frictional behavior of the suspensions.

3.3 Particle deformability

The ball bearing mechanism is strongly dependent on the ability of a particle to retain its spherical shape during rolling and sliding. The results in the previous section already indicated that the load applied on each individual sphere influences the frictional behaviour: particles that are more likely to deform give higher friction coefficients. When particles deform into an ellipsoidal shape, the contact area between the particles and the glass and PDMS surface increases, which limits rolling of the particles and sliding of the surfaces. To examine how the deformability of soft spheres influences their ball bearing-ability, we have varied the stiffness of the gelatin hydrogel particles in suspension. This was done by using a range of gelatin concentrations (10 to 20%) in the initial solution used to make the gelatin-in-oil emulsion, which consequently altered the gelatin content in the hydrogel particles. As it is challenging to measure the modulus of a single soft particle on a micrometer scale, we measured the Young's modulus of macroscopically large gelatin disks of similar gelatin concentration. The Young's moduli for gels with different gelatin concentrations are given in Fig. 7a. The suspension packing fraction used in all these experiments, was "100%" as previously defined. As the volume fraction of particles in the suspension is assumed to be
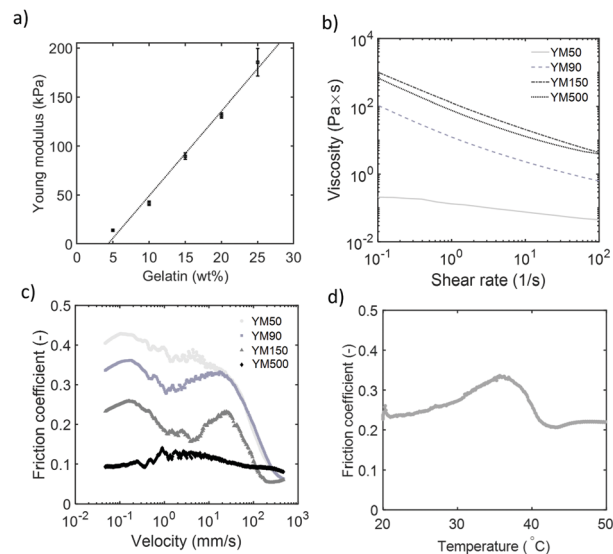
the same, but the gelatin concentration within the particles differ, the total gelatin concentration of the suspension should also change proportionally.

3.3.1 Particle characterisation. To confirm that the suspensions of different gelatin microparticles indeed had a similar volume fraction, we measured the dry weight of the particle suspensions. After evaporating the water from the suspensions overnight, we found that the dry gelatin content in 20% gelatin particle suspensions was twice as high as found for the 10% particle suspension. We therefore assume that the gelatin microparticles indeed contained the desired gelatin content, i.e., no deviating particle swelling or shrinking occurred, and that the Young's moduli of the particles in the suspension are well represented by the moduli of the macroscopic gels. The different particles had a similar particle size ranging from 5 to 11 μm, where the particles with a higher gelatin content were slightly larger than the ones with low gelatin content. We assume that the relatively small differences in average particle size have a limited effect, and that these particles thus mainly vary in their deformability. An additional sample with particles with a much higher stiffness was obtained by chemically cross-linking the 15 wt% gelatin samples using glutaraldehyde. The Young's modulus of the chemically cross-linked samples (YM500) is 0.5 kPa as we described elsewhere.[2] This value is a factor five higher than the modulus for the original 15 wt% gelatin gel (YM90). The chemical cross-linking of gelatin did not change the particle size (Table 2). The viscosity profile of these particle suspensions with particles with different Young's moduli (YM) are shown in Fig. 7b. As can be seen, the viscosity increased for stiffer particles, although the difference in viscosity between samples with particles of Young's modulus 150 kPa and 500 kPa was limited.

3.3.2 Friction depends on particle modulus. The tribological data of the suspensions with particles varying in deformability are displayed in Fig. 7c as a function of velocity. The softest particles with a low modulus of 50 kPa (YM50) show the highest friction coefficients especially at lower velocities. We find that the friction coefficient decreases with decreasing particle deformability (increasing modulus). The lowest friction coefficients are found for the stiffest particles (YM500). These stiff particles are able to provide a low friction coefficient of around 0.1 already in the boundary regime. These results strongly suggest that deformability is a main contributor to the differences in frictional behavior, especially for lower velocities, *i.e.* boundary regime. In literature, it is often argued that in the boundary regime the gap size is too narrow for particle entrapment, and that friction is mainly dominated by the continuous fluid phase.[21,26] In our case, we measure distinctly different friction coefficients in regime I. For the softest particles, we find $\mu_{\text{regime I}} \approx 0.4$ and for the hardest particles we find $\mu_{\text{regime I}} \approx 0.1$, even though the continuous fluid phase is the same. It thus appears that particles are already present between the surfaces at low velocities (regime I or boundary regime). The continuous aqueous phase would give relatively high friction coefficients in this regime, therefore water alone cannot be responsible for lubricating the surfaces in the first regime.

3.3.3 Interpreting the frictional curves. The suspensions containing softer particles give higher friction coefficients and appear to be less able to act as ball bearings. We expect these particles to be deformed easily during compression and shear, leading to a more ellipsoidal shaped particle. Due to this geometrical change, the particles have a decreased rolling ability, limiting the mobility of the glass-PDMS contact surfaces. This leads to high friction coefficients for the soft particles. For the stiffer, chemically cross-linked samples (YM500), the particles are hard enough to retain their spherical shape under the applied load, which gives low friction coefficients over the entire velocity range (Fig. 7c). We also see that these particle suspensions do not display the four regimes we previously observed. Instead, the friction coefficient remains rather constant over the entire velocity range. The four regimes are clearly present for the softer YM90 and YM150 particles, and there is a clear mixed regime present at higher velocity, recognized by the steep decrease in friction coefficient. For the softest YM50 particles however, the second and third regime are less pronounced. This is probably due to differences in the gap size as a result of the deformation of the particles. The deformation of the particles (δ) can be approximated with Hertzian-type contact mechanics, adapted to the deformation of soft spheres (eqn (2)).[39,40]

$$\delta = \left[\frac{3(1-\nu^2)}{4ER^{1/2}} \right]^{2/3} F_N^{2/3} \qquad (2)$$

In this equation E is the Young's modulus of the particles, F_N is the applied load, R is the diameter of the particles and ν is the Poisson ratio. Here, we assume a value for ν = 0.5 for incompressible materials.[41] From the light wear track observed on the PDMS pins after measurements, we estimate the total contact area between the glass ball and the three PDMS pins to be 7 mm². Using the average particle sizes, we estimate the force per particle: the deformation for the hardest particles with a Young's Modulus of 500 kPa is then around 24% while the softest particles are fully flattened with calculated values over 100% deformation with respect to their original size. To more accurately calculate these values, the exact number of particles present between the surfaces needs to be known at each velocity, as well as the number of lubricating layers. It is however currently not possible for us to measure these characteristics *in situ*. Additionally we need to take into account that the equation used here does not include the roughness of the surfaces, which may alter the exact contact area and with that the number of particles. With the current estimation, however, we do get a better perception of the difference in deformation between hard and soft particles.

When the particles are flattened to a larger extent, the gap size remains small, and the surfaces come in closer contact. This explains the high friction coefficients found for the softest hydrogel particles and the absence of four distinct frictional regimes.

Thus far we have found that the multiple regimes disappear in two cases: (1) when the particle number is small or the particles are too soft to separate the surfaces, leading to glass-PDMS contact, and (2) when the particles are hard enough to continuously separate the surfaces under the applied load. In the first case there is a high degree of constant contact between the surfaces, while the latter case describes a situation where the surfaces are at distance with low degree of contact over the entire velocity range. It seems that the regimes are visible when there are fluctuations in contact (area) between the glass ball and the PDMS pins instead of continuous contact or separation.

3.3.4 The role of effective suspension viscosity. To ensure that the differences in friction coefficients are caused by surfaces properties and not by bulk or rheological properties, we measured the viscosity of our samples as shown in Fig. 7b. For many lubricants, a high viscosity is thought to allow the creation of a stable film to avoid direct contact between the entraining surfaces and as such decrease friction,[42,43] or to shift the regimes commonly observed on the Stribeck curve. Here, we find similar viscosities for the YM150 and YM500 samples, with the latter showing a slightly lower viscosity (Fig. 7b). The YM500 suspension with the lower viscosity, however, gives much lower friction coefficients and different friction dynamics with a rather monotonous curve. In the case of our particle suspensions, the viscosity is therefore not responsible for the differences in frictional behavior. Instead, the characteristics of the rolling particles likely play the most important role when it comes to lubrication.

3.3.5 Melting particles. We change the particle deformability *in situ* by changing the temperature during a constant rate tribological test. To test the temperature dependence, we performed measurements at a fixed velocity of 50 mm s⁻¹ and 1 N while we gradually increased the temperature from 20 to 50 °C (Fig. 7d). As the temperature increases, the thermosensitive gelatin particles become softer as the gelatin network destabilizes. This process continues until a polymer solution is obtained at

around 40 °C due to disruption of hydrogen bonds responsible for the network formation. During initial stages, when the temperature increases from 20 to 35 °C, the friction coefficient increases from around 0.25 up to 0.33. As the particles become softer at higher temperatures, the particles easily deform, making them less able to roll and keep the surfaces apart. When the temperature further increases, the particles start to melt, which decreases the particle size and stiffness even further. This reduces the rolling ability and leads to an increase in friction. Above 37 °C, we observe a decrease in the friction coefficient. This is above the melting temperature for the type of gelatin used here.[44] Upon melting, the gelatin network collapses and the particles completely disintegrate, turning the suspension into a gelatin solution. We thus exploit the low melting point of gelatin to test the role of particles in lubrication. A transition occurs from a ball bearing type mechanism to a simple fluid film separating the surfaces as was seen in Fig. 4. Once the fluid film has formed, a friction coefficient of 0.23 is obtained. A closer look at Fig. 7d reveals more fluctuations in the friction coefficient at low temperatures, when the particles are still solid. Solid particles can be expected to give changes in gap size as particles enter and exit the gap. This explains why fluid samples give smoother frictional curves. The peak in frictional values for the softened particles around 35 °C strengthens our hypothesis that the ball bearing ability is decreased with decreased particle stiffness.

3.4 Particle size influences the friction coefficient

From previous sections it appears that the friction coefficient is determined by the ability of the soft spherical particles to keep the sliding surfaces apart. Here, we try to vary the distance between the surfaces by using particles of different sizes. We prepared hydrogel particles of different average sizes by varying the mixing speed when making the initial gelatin-in-oil emulsion (Table 1). We have labelled the samples based on the $D[4,3]$ average radii of the particles: small (12 μm), medium (33 μm) and large (150 μm). The particles were made with 15% gelatin and the particle suspensions were prepared at the maximum packing fraction (100%). The friction coefficients of the hydrogel particle suspensions, with particles varying in size, are shown in Fig. 8a. Measured particle size distribution and viscosity profiles of the suspensions can be found in Fig. 8b. By varying the particle sizes,

we find differences in the actual friction coefficients and more importantly, in the overall frictional behavior. The viscosity profiles of these particle suspensions however, only show minor differences (Fig. 8b). This again shows that the viscosity is not a main contributor to the frictional behavior observed here.

We find the lowest friction coefficients for the largest particles beyond the boundary regime. This was expected as large particles are able to keep the surfaces at a larger distance, leading to minimal direct contact between the surfaces. However, the low friction coefficient for the large particles is only observed after a velocity of around 5 mm s^{-1}, and the suspension does not transition through the four frictional regimes. The suspensions with small and medium sized particles (12 and 33 μm respectively) do display the frictional curves consisting of the four regimes, as expected based on the previous results.

3.4.1 Surface–particle interactions. In the first lubrication stages, the largest particles and smallest particles show similarly high friction coefficients. For the small particles this may be caused by asperity contact between the glass ball and PDMS pins. Atomic force microscopy of the PDMS surface showed that the peak height and width of the surface asperities was around 500 nm, much smaller than the size of the particles. The surface roughness of the glass probe is shown in Fig. 9. These asperities are mostly larger than the smallest particles (12 μm). These small particles are therefore small enough to be trapped between the surface asperities of the glass ball. The entrapped particles would then be unable to separate the surfaces, that results in a high degree of asperity contact between the substrate and the probe. This makes these small particle suspensions a less efficient ball bearing lubricant. The large particles with an average size of 150 μm also show lower lubricating ability in the boundary regime. As the large particles are expected to be larger than the surface asperities of the glass ball and PDMS pins, these particles are not trapped between asperities and do have the ability to separate the surfaces. Due to the larger particle size, however, fewer particles fit on the same surface area, which increases the applied load per particle. Under this relatively high load, these particles may be deformed to a more elliptical shape. Using eqn (2), we estimate the large particles (150 μm) to be deformed to a final height of 35 μm. This deformation reduces the lubricating properties as the contact area between the particles and the surfaces increases and the rolling ability decreases. Although the deformed large particles have a similar height (35 μm) as the size of the medium particles (33 μm), the friction coefficient for the medium particle suspensions is lower. This can
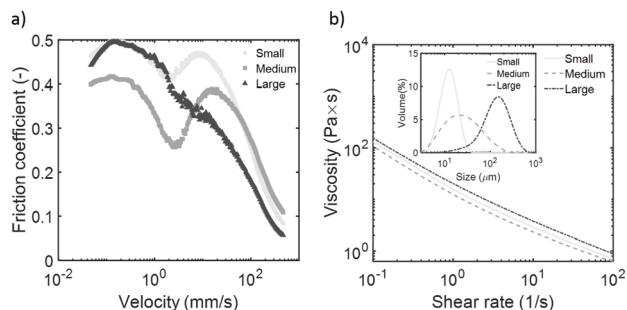

Fig. 8 Friction coefficients (a) and flow curves (b) obtained for suspensions with microparticles with varying particle sizes. Inset shows the particle size distribution. Particle characteristics can be found in Table 2.
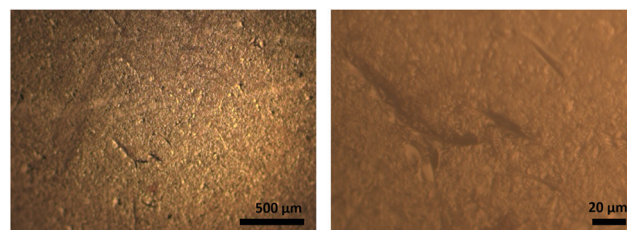

Fig. 9 Microscopy image of the spherical glass probe, showing the relatively high degree of roughness of the surface.

be explained by the number of particles. The number of medium-sized particles is at least 100 times larger than the number of the large particles. The expected load per medium particle is therefore much smaller than for the large particles and as a result the deformation of these particles is also expected to be smaller. The medium-sized particles therefore remain mostly spherical. We attribute the low friction coefficients of the medium particles thus to their ability to roll due to a lower deformation, and inability to be trapped between surface asperities. These results show that there is an optimum in particle properties; they should be small enough to provide a large number of particles that do not deform, but they should be large enough not to get trapped within the asperities. This makes the suspension with the medium particles an efficient ball bearing lubricant, especially in the first regimes as shown in Fig. 8a.

3.4.2 Frictional regimes for different particle sizes. Both the medium-sized (33 μm) and small particles (12 μm) show the four frictional regimes as described in previous sections. For the large particles, the frictional behavior is noticeably different and the four regimes are less pronounced. Specifically the increase in friction in regime III is absent. The phenomenon responsible for the increase in friction thus does not occur in suspensions with large particles as the increase in friction expected for the third regime is not seen here. In regime IV, the last regime, the friction coefficient becomes smallest for the large particles. In this regime, we assume that a large amount of particles can be present between the surfaces as the gap size increases. As the large particles are well able to keep the surfaces at a relatively large distance, these low friction coefficients are to be expected. Again we find that the low friction coefficients are obtained with particles that are able to act as ball bearings by keeping a distance between surfaces while rolling over the surfaces easily, regardless of the rheological properties of the suspension.

3.5 Interpretation of soft particle lubrication

For soft ball bearing systems, small particles, soft particles and a low volume fraction of particles in suspension leads to relatively high friction coefficients. On the other hand, low friction is found for hard, large particles and when particles are present in large amounts. The systems with high friction coefficients have an important characteristic in common: a poor ability to separate surfaces and particles with a low ability to roll. These aspects are of high importance for the ball bearing mechanism. Instead of the well-known three regimes, *e.g.* boundary, mixed and hydrodynamic regime, our particle suspensions transition through four frictional regimes. Similar frictional zones have been found before for lubricants containing solid-like particles.[21,26] We have shown the importance of the particle properties in the occurrence of the different frictional regimes. When particles are too soft, too hard or too large, the particle suspensions do not transition through all four frictional regimes.

Based on our findings with systematic variations in particle properties, we provide new insights regarding the interpretation of the different frictional regimes for soft particles in a fluid matrix. In previous works, it was suggested that high friction arises from low particle number entrainment,[21,26] due to a large

particle size compared to the gap size or as a result of local build-up of particles around the probe.[27] However, we find different friction coefficients for all of our samples in the boundary regime or regime I, and the most solid-like, chemically cross-linked particles are unaffected by the changes in gap size (Fig. 7). This strongly indicates that particles are already present between the sliding surfaces, even at relatively small gap sizes at low speeds. High friction coeffficients are therefore expected to arise from deformation of the soft particles. Low friction coefficients are then found when the particles are spherical and able to roll. The increase in gap size will also lead to the presence of a large amount of particles, collectively acting as a good lubricant due to good rolling ability and large separation of the surfaces. As the particles have less contact with the surfaces, the properties of the particles become less relevant. Based on these observations, we therefore propose the following lubrication mechanisms for the four different regimes for soft hydrogel particle suspensions between rough surfaces (Fig. 10):

Regime I. At these small gap sizes, a limited number of particles is present between the surfaces, and depending on their size, the particles may become trapped within the cavities on the rough glass surface (Fig. 9) carrying relatively high loads. The compressed particles lose their spherical shape and rolling ability and are dragged along the PDMS surface. In this case, relatively large contact areas between the glass and PDMS surfaces are expected, leading to rather high friction coefficients in this boundary regime.

Regime II. As the velocity increases, the gap size increases. More particles enter between the glass-PDMS surfaces and the deformable particles regain their original spherical shape. The improved rolling ability of the particles provides sufficient lubrication and gives rise to a decrease in the friction coefficient until a certain minimum value where the particles are assumed to be completely spherical.

Regime III. At even higher velocities, the change in friction coefficient can be attributed again to geometrical changes of the particles during sliding. As the velocity increases in
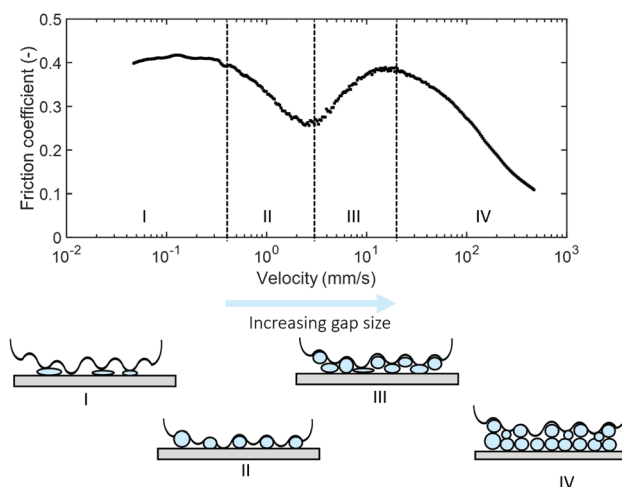

Fig. 10 Schematic representation of our proposed four frictional regimes of hydrogel microparticle suspensions as the velocity and gap size increase.

regime III, more space between the PDMS and glass surfaces is created, probably at a distance comparable to or larger than the particle size. Such an increase in gap size leads to an inflow of more particles. An excess of particles between the surface may lead to jamming of the particles, compression of particles, and perhaps even the formation of multiple lubricating layers. All effects would limit the ability for the particles to roll, hence an increase in the friction coefficient is expected.

Regime IV. In the mixed regime, the gap size is thought to further increase. Firstly, this causes the layered particles to regain their original shape and rolling ability. Secondly, this makes it possible for more particles to enter the gap quickly as the velocity increases. The suspension can now form a viscous lubricious layer where direct contact between the surfaces and the particles is reduced. The ball bearing mechanism becomes less relevant, and lubrication by a fluid film becomes more dominant. The strong decay in friction coefficient in the mixed regime (regime IV) is typical for rate-dependent frictional curves and shows similarities to a gelatin solution or water (Fig. 4).

We summarize our proposed mechanism schematically in Fig. 10.

This mechanism highlights the important role of the particle properties combined with the surface properties on the lubrication behavior of hydrogel particle suspensions. We point out the importance of the deformable nature of the particles for the appearance of the specific behavior observed in regime II and III. These regimes are absent for particles that are less sensitive to deformation. For small particles we find high friction, likely because particles are trapped between surface asperities.

3.6 Smooth surface lubrication

To demonstrate the importance of particle trapping within the surface asperities, we carried out measurements using a smooth steel ball instead of the rough glass ball, as this allows us to study the effect of surface properties. For this polished steel ball we expect the surface asperities to be far smaller than our particles which are several micrometers in size. Particle trapping will thus be less probable in the case of this smooth steel ball. Indeed our measurements performed with the smooth steel ball show different rate-dependent lubrication behavior than previously seen; the frictional regimes observed when using a smooth steel ball are different from those seen for the glass ball (Fig. 11). For the rough glass ball we related the decrease in the second regime and increase in third regime to particle trapping and deformation. The steel ball, however, shows a rather steady decrease in friction coefficient in regime II and III. It thus appears that the fluctuations in particle trapping that result in changes in contact between the sliding surfaces are different for a smooth ball. Aside from the different frictional regimes, the steel ball also seems to display higher friction coefficients for the majority of the measured velocities. With the smooth ball, less particles are being trapped between the surfaces meaning more particles are excluded from the sliding interface. This leads to more contact between the steel ball and the PDMS surface resulting in higher friction coefficients. The smooth ball has a larger contact area with the PDMS surface than a rough
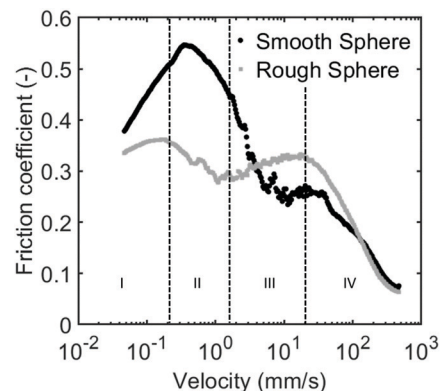

Fig. 11 Frictional curves of hydrogel particles of 90 kPa measured with a smooth steel ball and a rough glass ball against relatively smooth PDMS pins. Lines are placed at the transition points for the rough glass ball.

ball where only several asperities are in contact with the flat substrate. Sliding experiments with PDMS using rough surfaces have shown lower friction coefficients compared to friction with smooth surfaces[45,46] which is also observed here. This decrease in friction is likely due to relatively high adhesive forces of PDMS.[47] In addition, with the smooth ball, less particles could be trapped between the surfaces meaning more particles are excluded from the sliding interface. This leads to more contact between the steel ball and the PDMS surface resulting in higher friction coefficients. By varying the surface properties and the particle properties we have shown how the complex frictional behavior of particle suspensions depends on both the properties of the lubricant and the surface properties of the interacting bodies.

4 Conclusions

In this work we elucidate how and why soft hydrogel particle suspensions act as good lubricants. We find four frictional regimes as a function of velocity. By systematically exploring the relevant physical characteristics of particles and surfaces involved we can propose a physical lubrication mechanism for each regime observed. We identify variations in gap size and particle deformability as the main cause for the rate-dependence observed. We show that when a large degree of contact between the interacting surfaces is to be expected (presence of small, soft and limited number of particles), large friction coefficients are obtained. Low friction coefficients are measured when particles diminish surface–surface interaction, and in addition, easily roll over the surfaces. This is the case for large particles, hard particles and particles present in high volume fractions. Additionally, we show that different surface characteristics give way to entirely different friction dynamics. Our hydrogel particle suspensions are thus efficient lubricants and are also a useful model system to better interpret the complex frictional behavior of soft materials.

Conflicts of interest

The authors declare that there are no conflicts of interest.

Acknowledgements

Notes and references

1 J. M. Urueña, E. O. McGhee, T. E. Angelini, D. Dowson, W. G. Sawyer and A. A. Pitenis, *Biotribology*, 2018, **13**, 30–35.
2 R. E. D. Rudge, E. Scholten and J. A. Dijksman, *Tribol. Int.*, 2019, 105903.
3 D. Berman, A. Erdemir and A. V. Sumant, *Mater. Today*, 2014, **17**, 31–42.
4 S. Biswas and K. Vijayan, *Wear*, 1992, **158**, 193–211.
5 R. K. Upadhyay and L. A. Kumaraswamidhas, *Handbook of Materials Failure Analysis*, Elsevier, 2018, pp. 209–233.
6 K. Liu, Y. Tian, M. Stieger, E. van der Linden and F. van de Velde, *Food Hydrocolloids*, 2016, **52**, 403–414.
7 K. Johnson, *Proc. – Inst. Mech. Eng.*, 1959, **173**, 795–810.
8 F. Deng, G. Tsekenis and S. M. Rubinstein, *Phys. Rev. Lett.*, 2019, **122**, 135503.
9 S.-H. Yue, *Rotating cup mechanism*, US Pat. 6719451, 2004.
10 E. Videira, C. Lebreton, S. Lewis and L. Gaillard, 15th European Space Mechanisms and Tribology Symposium-ESMATS, 2013.
11 R. Stribeck, *Z. Ver. Dtsch. Ing.*, 1902, **46**, 1341–1348.
12 J. P. Gong, T. Kurokawa, T. Narita, G. Kagata, Y. Osada, G. Nishimura and M. Kinjo, *J. Am. Chem. Soc.*, 2001, **123**, 5582–5583.
13 J. P. Gong, *Soft Matter*, 2006, **2**, 544–552.
14 M. Workamp and J. A. Dijksman, *J. Rheol.*, 2019, **63**, 275–283.
15 M. Bahrami, V. Le Houérou and J. Rühe, *Tribol. Int.*, 2019, DOI: 10.1016/j.triboint.2019.02.045.
16 A. Pitenis, J. Urueña, K. Schulze, R. Nixon, A. C. Dunn, B. Krick, W. Sawyer and T. Angelini, *Soft Matter*, 2014, **10**, 8955–8962.
17 J. Klein, E. Kumacheva, D. Mahalu, D. Perahia and L. J. Fetters, *Nature*, 1994, **370**, 634.
18 X. Banquy, J. Burdynska, D. W. Lee, K. Matyjaszewski and J. Israelachvili, *J. Am. Chem. Soc.*, 2014, **136**, 6199–6202.
19 J. Gong, M. Higa, Y. Iwasaki, Y. Katsuyama and Y. Osada, *J. Phys. Chem. B*, 1997, **101**, 5487–5489.
20 Y. A. Meier, K. Zhang, N. D. Spencer and R. Simic, *Langmuir*, 2019, **35**, 15805–15812.
21 A. Gabriele, F. Spyropoulos and I. Norton, *Soft Matter*, 2010, **6**, 4205–4213.
22 A. Sarkar, F. Kanti, A. Gulotta, B. S. Murray and S. Zhang, *Langmuir*, 2017, **33**, 14699–14708.
23 Y. Wu, T. Tang, B. Bai, X. Tang, J. Wang and Y. Liu, *Polymer*, 2011, **52**, 452–460.
24 E. Andablo-Reyes, D. Yerani, M. Fu, E. Liamas, S. Connell, O. Torres and A. Sarkar, *Soft Matter*, 2019, **15**, 9614–9624.
25 S. Lee, M. Heuberger, P. Rousset and N. D. Spencer, *Tribol. Lett.*, 2004, **16**, 239–249.
26 P. T. Nguyen, O. Kravchuk, B. Bhandari and S. Prakash, *Food Hydrocolloids*, 2017, **72**, 90–104.
27 I. F. Farrés and I. Norton, *Food Hydrocolloids*, 2015, **45**, 186–195.
28 B. Zhang, N. Selway, K. J. Shelat, S. Dhital, J. R. Stokes and M. J. Gidley, *Carbohydr. Polym.*, 2017, **155**, 128–135.
29 R. E. D. Rudge, E. Scholten and J. A. Dijksman, *Curr. Opin. Food Sci.*, 2019, **27**, 90–97.
30 H. M. Shewan, C. Pradal and J. R. Stokes, *J. Texture Stud.*, 2020, **51**, 7–22.
31 G. Scott and D. Kilgour, *J. Phys. D: Appl. Phys.*, 1969, **2**, 863.
32 G. Cassin, E. Heinrich and H. Spikes, *Tribol. Lett.*, 2001, **11**, 95–102.
33 R. Gallego Calvo, T. Cidade, R. Sánchez Martnez, C. Valencia Barragán, F. Gómez and J. Mara, *et al.*, *Tribol. Int.*, 2016, **94**, 652–660.
34 T. Shoaib, J. Heintz, J. A. Lopez-Berganza, R. Muro-Barrios, S. A. Egner and R. M. Espinosa-Marzal, *Langmuir*, 2017, **34**, 756–765.
35 K. Bett and J. Cappi, *Nature*, 1965, **207**, 620–621.
36 N. Selway and J. R. Stokes, *Food Res. Int.*, 2013, **54**, 423–431.
37 E. D. Bonnevie, D. Galesso, C. Secchieri, I. Cohen and L. J. Bonassar, *PLoS One*, 2015, **10**, e0143415.
38 A. Oppermann, L. Verkaaik, M. Stieger and E. Scholten, *Food Funct.*, 2017, **8**, 522–532.
39 K. Kim, J. Cheng, Q. Liu, X. Y. Wu and Y. Sun, *J. Biomed. Mater. Res., Part A*, 2010, **92**, 103–113.
40 P. Ding, I. Norton, Z. Zhang and A. Pacek, *J. Food Eng.*, 2008, **86**, 307–314.
41 K. S. Anseth, C. N. Bowman and L. Brannon-Peppas, *Biomaterials*, 1996, **17**, 1647–1657.
42 J. Bongaerts, K. Fourtouni and J. Stokes, *Tribol. Int.*, 2007, **40**, 1531–1542.
43 J. M. Kim, F. Wolf and S. K. Baier, *Tribol. Int.*, 2015, **89**, 46–53.
44 I. Haug and K. Draget, *Handbook of food proteins*, Elsevier, 2011, pp. 92–115.
45 J. Yu, S. Chary, S. Das, J. Tamelier, K. L. Turner and J. N. Israelachvili, *Langmuir*, 2012, **28**, 11527–11534.
46 B. He, W. Chen and Q. J. Wang, *STLE/ASME 2006 International Joint Tribology Conference*, 2006, pp. 1053–1062.
47 E. Kroner, R. Maboudian and E. Arzt, *Adv. Eng. Mater.*, 2010, **12**, 398–404.